THE JOURNAL OF PHYSICAL CHEMISTRY C
A JOURNAL OF THE AMERICAN CHEMICAL SOCIETY

pubs.acs.org/JPCC

Article

Modulation Effect of Substrate Interactions on Nucleation and Growth of MoS_2 on Silica

Nadire Nayir, Stephen Bartolucci, Tao Wang, Chen Chen, Joshua Maurer, Joan M. Redwing, and Adri C. T. van Duin*

Cite This: *J. Phys. Chem. C* 2023, 127, 9039−9048

Read Online

ACCESS | Metrics & More | Article Recommendations | Supporting Information

ABSTRACT: Chemical vapor deposition is a well-established bottom-up technique to produce a high-quality single-crystal MoS_2 film. In this technique, the substrate (e.g., silica) plays a crucial role in the segregation and chemical interaction of precursors to form grain-sized MoS_2. However, the mechanisms of the surface interactions that influence the properties of MoS_2 during growth are still poorly understood. Here, we combine ReaxFF reactive molecular dynamics simulations, density functional theory (DFT) calculations, and experimental growth of MoS_2 to provide an atomic insight into the coupling between the surface chemistry and the MoS_2 nucleation and growth on a silica surface. Our experimental results show that the dehydroxylated surface stays mainly inert during the MoO_3 flow, while the presence of hydroxyl groups leads to MoO_3 nucleation on the substrate. ReaxFF and DFT simulations further confirm that the reaction between MoO_3 and the hydroxylated surface is both thermodynamically and kinetically driven, indicating that hydroxyl groups formed on silica enhance the chemical reactivity of the surface toward MoO_3 molecules and promote the growth. Additionally, the MoS_2 growth on the hydroxylated silica support initiates with MoO_3 nucleation followed by the chalcogen−surface interactions. Moreover, the existence of the substrate catalyzes the growth by lowering the growth temperature, providing an effective way for energy saving and cost reduction. These results demonstrate the intricate role of surface engineering in controlling and promoting large-area MoS_2 growth.

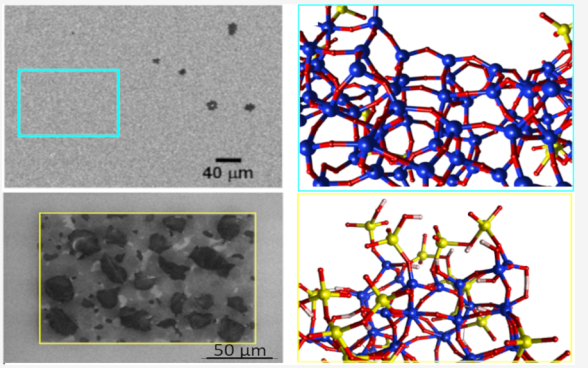

1. INTRODUCTION

MoS_2 is one of the most studied transition metal dichalcogenides, owing to its exceptional electronic and optoelectronic properties.[1−5] Atomically thin MoS_2 experiences weak interlayer van der Waals interactions but strong in-plane covalent bonding; therefore, it can be synthesized either by top-down[6−9] or bottom-up approaches.[10−15] Top-down approaches essentially rely on breaking van der Waals bonds between interlayers to exfoliate a single or few-layered two-dimensional (2D) material from the bulk form, which comes at the cost of sacrificing crystal quality. Alternatively, bottom-up approaches are well-advanced growth techniques, which utilize precursors in either the gas or solid phase, to grow large-area high-quality single-crystal MoS_2. With bottom-up techniques, atomic or molecular precursors react to form individual crystal grains and then coalesce into a single layered thin film. Chemical vapor deposition (CVD)[11,14−20] is one of the most used bottom-up growth techniques to produce a thin layer of 2D MoS_2. This technique makes use of a substrate whose surface chemistry and orientation play a crucial role in the segregation and chemical interaction of precursors to form 2D MoS_2. The existence of high adsorption sites on the surface drives precursor/surface interactions that lead to the growth of 2D domains on the surface.[21,22] Additionally, the sulfurization of metal-oxide or organometallic precursors in the CVD environment has been adopted as a common approach to produce an atomically thin, large-area MoS_2. MoO_3 has been regarded as a suitable metal oxide precursor owing to its moderate melting and vaporization points.[11,14,23−28]

Due to its high melting temperature, low cost, and high surface quality, previous works have demonstrated that silica is an ideal substrate for the growth of MoS_2.[14,16,29−31] Additionally, progress in the synthesis of MoS_2 on silica has revealed the impact of the surface chemistry of the substrate on the growth of MoS_2, which has directed attention toward the surface engineering of the substrate to enhance the growth and crystal quality of MoS_2.[14,16,32,33] In particular, Bartolucci et al.[14] demonstrated that Ga^+ ion bombardment is an effective way to generate isolated surface hydroxyl groups. The Ga-treated

Received: February 14, 2023
Revised: April 22, 2023
Published: May 9, 2023

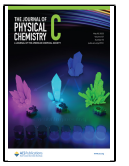

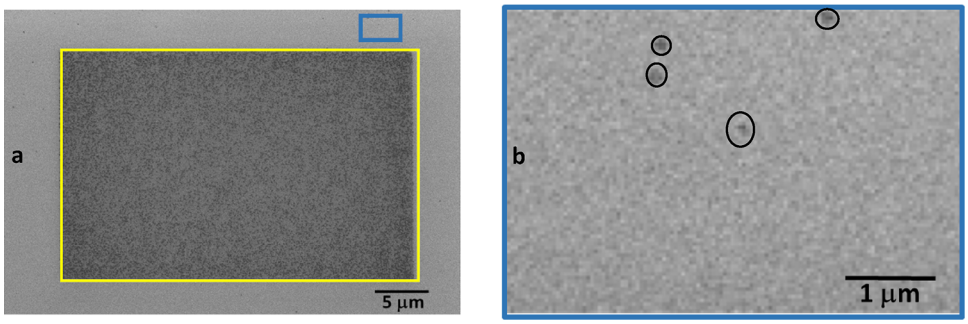

Figure 1. Ga^+ ion beam-induced MoS_2 growth. (a) SEM image of patterned growth of MoS_2, where the region indicated by the yellow rectangle was irradiated with a Ga^+ ion dose of 4.58×10^{15} ions/cm^2. (b) Outside the Ga-treated pattern (enclosed by the blue rectangle) where there are no discernable features except for a few crystals of MoS_2 on the substrate (highlighted with black circles).

surface resulted in higher MoS_2 nucleation compared to the non-Ga-treated surface due to the increase in the concentration of −OH functional groups attached to the surface.[14] However, it is also reported that Ga^+ ion beam irradiation induces surface damage and contamination with Ga residues, which can affect the nucleation and growth of MoS_2.[34] All these scientific improvements have resulted in the need for an atomic-level understanding of the surface interactions between MoS_2 and silica and thus have prompted the development of cost-effective multiscale models. Tsafack et al.[35] uncovered the molecular mechanism of the MoO_3 sulfurization at the DFT level. They proposed reaction pathways for the formation of experimentally observed intermediates of MoS_2O and MoO_2S, which are expected to lead to the end product of MoS_2. As a follow-up study, Tsafack et al.[36] also reported a joint ReaxFF and DFT investigation of the chemical reactions of S_2 and/or S_3 with MoO_3, but they demonstrated that the ReaxFF potential[37] lacks information required for understanding the CVD growth of MoS_2 from MoO_3 and S_2 or H_2S precursors.

Using the combination of analysis of experimental growth of MoS_2, ReaxFF MD simulations, and density functional theory (DFT) calculations, this work studied the impact of the surface chemistry of silica on the MoS_2 growth. To accurately model the phenomenon observed in experiments, we developed a ReaxFF potential, which is capable of simulating the CVD growth of MoS_2 from MoO_3 and S_2 or H_2S precursors and other chemical reactions. The details of the force field development can be found in the Supporting Information (SI).

2. THEORETICAL SECTION

2.1. ReaxFF Reactive Force Field. ReaxFF, originally developed by van Duin et al.,[39] is a bond order and charge-dependent potential force field. It updates interatomic distance and bond order at each iteration, thereby creating a chemically reactive environment. Since the CVD growth of materials requires high energy and a chemically reactive environment, ReaxFF provides the accurate description of bond breaking and formation. The simplest form of the ReaxFF formalism can be given as below, and a detailed and most up-to-date form can be found in ref 40

$$E_{system} = E_{bond} + E_{angle} + E_{tors} + E_{Coulomb} + E_{vdW} + E_{over}$$

where E_{bond}, E_{angle}, and E_{tors} are energy terms related to bond formation, three-body valence angle strain, and four-body torsional angle strain, respectively. The energy term E_{over} is used to prevent the overcoordination of atoms. The energy terms $E_{Coulomb}$ and E_{vdW} are associated with electrostatic and dispersive contributions, respectively. In the ReaxFF formalism, the force and energy contributions of bond order-dependent interactions such as the valence angle and dihedral angle disappear upon bond dissociation. The nonbonded terms associated with van der Waals and Coulomb interactions are computed at each molecular dynamics (MD) step regardless of connectivity. A Morse potential is employed in conjunction with a shielding term to accurately describe van der Waals interactions and prevent excessively high repulsion between atom pairs. For electrostatic energies, ReaxFF utilizes a shielded Coulomb potential. An electronegativity equalization[41] polarizable charge model allows the force field to derive atomic charges dynamically at each iteration to produce accurate and geometry-dependent charge distributions. To date, the ReaxFF method has been applied to a wide range of 2D materials.[37,42−50]

2.2. Molecular Dynamics Simulations. The ReaxFF force field used in this work was trained against a well-defined DFT-based training set, which describes the CVD growth of MoS_2 from MoO_3 and S_2 or H_2S precursors besides other chemical reactions. The force field development details can be found in the SI. MD simulations were run with a time step of 0.25 fs with periodic boundary conditions imposed in all three directions. A Berendsen thermostat[51] was utilized with a temperature damping constant of 100 fs with an NVT ensemble. In all MD simulations, the Verlet velocity algorithm was adopted to integrate the Newton equations of motion. ADF/ReaxFF simulation software[52] was deployed, and the simulation snapshots were generated with use of Open Visualization Tool (OVITO)[53] and VESTA.[54] For the preparation of amorphous silica with/without OH groups: 150 SiO_2 molecules were placed in a cubic simulation box with the dimension of 50 Å, then heated up to 1000 K with the rate of 0.005 K/ns, and equilibrated at 1000 K for 1 ns. After the equilibration, SiO_2 molecules condensed into an amorphous silica material, which consisted of nonpassivated oxidized (Figure 1a,e) and fully passivated siloxane (highlighted with blue dashed circles in Figures 1a, b, and f) regions. Then, the amorphous silica acquired from the last framework of the aforementioned simulation was exposed further to the H_2 gas-phase pressure at 1000 K for 1 ns after inserting 200 H_2 molecules into the simulation box with the dimension of 50 Å to obtain a hydroxylated silica surface (Figure 1b,g). For this, the vacuum around the amorphous silica was filled by H_2 molecules.

2.2.1. Treatment of Silica Only in MoO_3. Three models were constructed by exposing each silica substrate in Figure 1a−c to 50 MoO_3 gas-phase molecules in a simulation box with a dimension of 30 Å. Upon the structural minimization, each

https://doi.org/10.1021/acs.jpcc.3c01010
J. Phys. Chem. C 2023, 127, 9039−9048

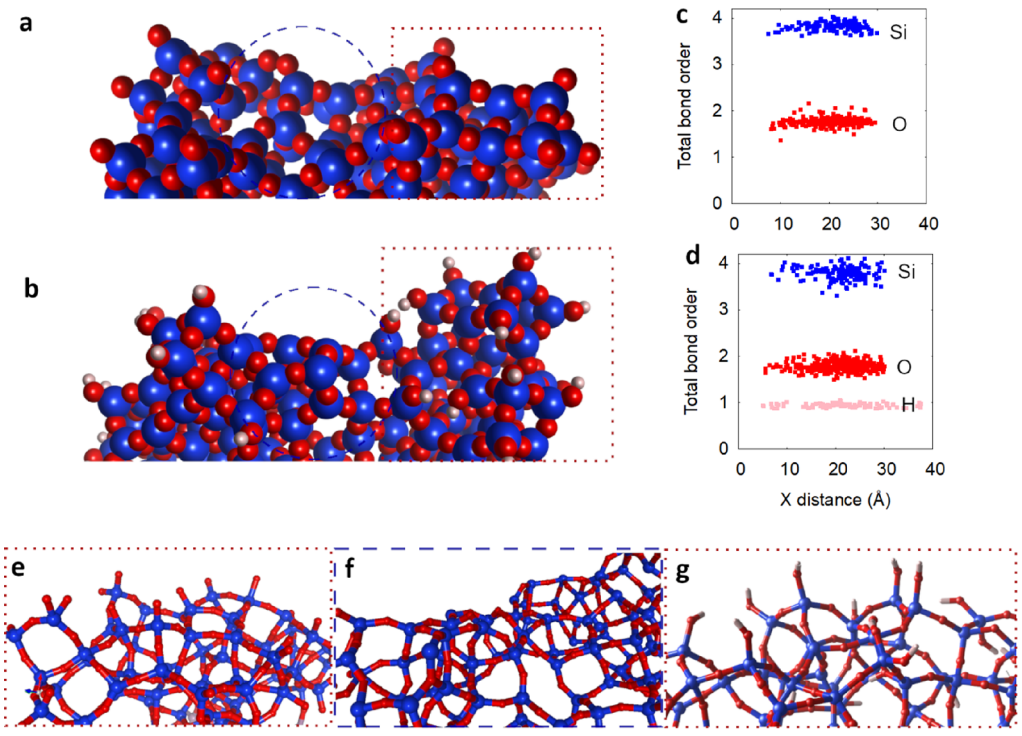

Figure 2. ReaxFF-computed amorphous silica (a) before and (b) after H_2 exposure and (c,d) associated total bond order distributions. (e) Magnified views of a nonpassivated oxidized silica surface (with a red dotted rectangle in a), (f) fully passivated siloxane (with a blue dashed circle in a and b), and (g) hydroxylated region (with a red dotted rectangle in b). Red, blue, and white balls represent O, Si, and H atoms, respectively.

model was heated up to 1000 K with a heating rate of 0.005 K/ps and then equilibrated for 1 ns. For treatment of silica only in S_2 or H_2S, two models were established by exposing the hydroxylated silica surface in Figure 1c to 200 S_2 and H_2S gas-phase molecules separately, in a simulation box with a dimension of 30 Å. Upon the structural minimization, each model was heated up to temperatures varying within the range of 1000−2000 K with a heating rate of 0.005 K/ps and then equilibrated for 2.5 ns. For treatment of silica in MoO_3 and S_2 or MoO_3 and H_2S together, 200 MoO_3 gas-phase molecules were inserted in a system that was exposed first to 200 S_2 and 200 H_2S, separately, at 1000 K for 2.5 ns in a simulation box with the dimension of 30 Å. Then, the mixed system was annealed further at the same temperature for 2.5 ns. For transition state searching, to explore the transition state of $O_3Mo\text{-}OHSi(OH)_3$, the bond length restraints were employed for bond O−H where atom O is from MoO_3 and H is from $Si(OH)_4$, for bond Mo−O with atom Mo from MoO_3 and atom O from $Si(OH)_4$, and for one H−O bond from $Si(OH)_4$ to drive the reaction during MD simulation to the structure of the product obtained from DFT.

2.3. DFT Calculations. Nonperiodic calculations of S_2 and H_2S molecules were performed via Jaguar[55] with the B3LYP functional and the LACV3P**++ effective core potential. The reaction path and the transition state between $O_3Mo\text{-}OHSi(OH)_3$ and $(OH)O_2Mo\text{-}OSi(OH)_3$ were explored using the nudged elastic band method implemented in SCM/AMS.[52,56] The calculations were performed with the general gradient approximation (GGA) with the PBE exchange and correlation functional.[57]

The binding energies of MoO_3 to three silica surfaces (Figure S3) were computed via VASP[58] with the use of projected augmented wave potentials.[59,60] The generalized gradient approximation in the scheme of Perdew−Burke−Ernzerhof[57,61] was paired with the zero-damped D3 dispersion correction.[62] A $30 \times 30 \times 30$ Å^3 simulation box with a vacuum layer of 15 Å was inserted along the three directions to avoid spurious interactions between replicas. The energy and force thresholds were set to 0.1 meV and 0.01 eV/Å. An energy cutoff of 400 eV and a Gaussian smearing width of 0.05 eV were used in the calculations.

3. EXPERIMENTAL SECTION

An FEI Helios Nanolab 600i dual-beam FESEM/ion beam was used to image and pattern the silicon with a 300 nm thermally grown oxide layer (University Wafer). Electron beam imaging was conducted at 10 kV. For patterning, the Ga^+ ion beam was operated at 30 kV at various beam currents. The ion dosage was calculated using the beam current, time, and area of the pattern. Two patterned regions with a lower (5×10^{15} ions/cm^2) and higher ion dosage (1.44×10^{16} ions/cm^2) were fabricated. Samples were typically exposed to ambient for several hours before MoO_3 growth. A microprocessor-controlled tube furnace (model 55053, Blue M, Thermo Scientific) with a one inch (25.4 mm)-diameter quartz tube was used for molybdenum trioxide seeding. The patterned wafer pieces were placed on a quartz boat facing down with 10 mg of MoO_3 powder (Sigma-Aldrich, >99.5%) placed at the upstream end of the boat. Argon was allowed to purge the tube for 20 min prior to heating. During growth, the argon flow was controlled at 20−50 sccm. The furnace temperature was set to 750 °C with a heating rate of 25 °C/min. The furnace temperature was held at 750 °C for 1 min and then allowed to cool slowly to room temperature. For S powder and H_2S treatment, the sulfur powder experiment was conducted with the same furnace parameters as described above except with the absence of MoO_3 powder and a soak time of 15 min. In addition, a second quartz boat filled with 0.5 g of sulfur powder (Acros, 99.5%) was placed on the upstream side of the

https://doi.org/10.1021/acs.jpcc.3c01010
J. Phys. Chem. C 2023, 127, 9039−9048

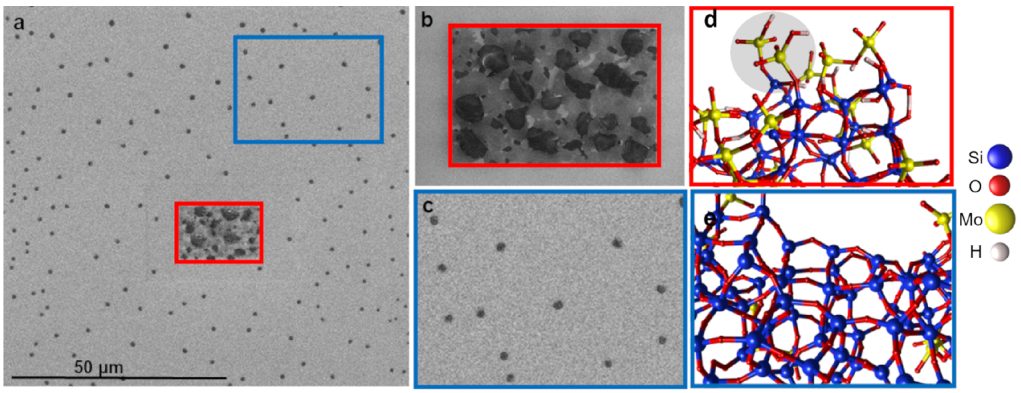

Figure 3. (a) Electron microscopy image of the Ga^+ ion-dosed silica surface and tube furnace growth at 750 °C for 1 min at the peak temp. with MoO_3 powder only. Maginifed views of (b) the rectangular pattern region created with an ion dosage of 5×10^{15} ions/cm^2 (indicated by the red rectangle in a) and (c) outside the pattern (highlighted with the blue rectangle in a). The ReaxFF snaphots taken from the simulations of MoO_3 exposed (d) hydroxylated and (e) fully passivated and dehydroxylated silica surfaces at 1000 K for 1 ns. The gray circle background in d highlights the MoO_x nucleation on the hydroxylated silica surface.

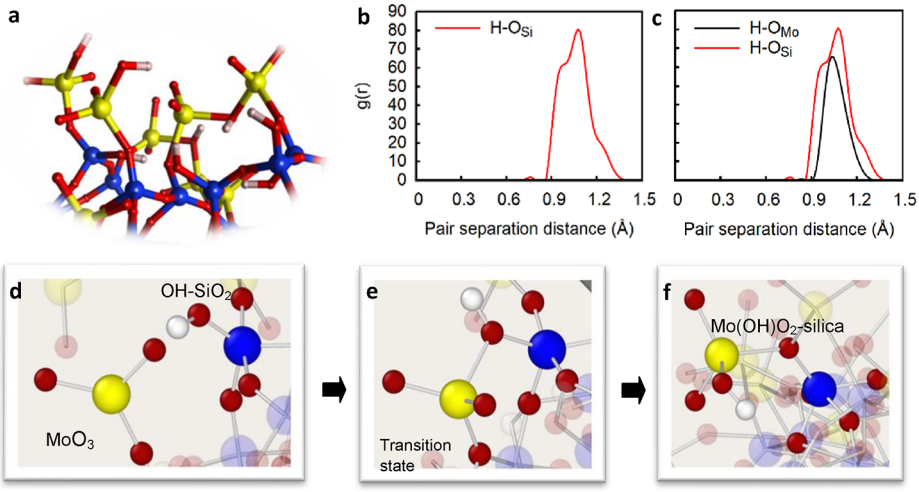

Figure 4. (a) MoO_3-exposed OH-silica surfaces at 1000 K for 1 ns and the partial radial distribution functions of H-O_{Mo} (O in a MoO_3 molecule) and H-O_{Si} (O on the silica surface) (b) before and (c) after MoO_3 exposure at 1000 K and H-O_{Mo} after exposure. (d–f) Protonation of MoO_3 in the proximity of the surface by H migration from the silanol group of the silica to MoO_3.

samples in the quartz tube under the heating tape. The heating tape was not turned on until the center of the furnace had reached 300 °C and was heated to 195 °C. In the H_2S exposure experiment, the Ga-implanted patterned SiO_2 sample was annealed in an MOCVD system by heating it up to 750 °C in N_2 ambient, then exposing the sample to 400 sccm H_2S gas flow with soaking for 5 min, and cooling down in N_2 to room temperature.

4. RESULTS AND DISCUSSION

Earlier studies[14,38] demonstrate that the hydroxylation of the silica surface drives MoS_2 nucleation. Ga^+ ion beam irradiation produces surface hydroxyl groups through a suggested mechanism by Bartolucci et al.,[14] which serve as points for volatile precursors to attach to the surface. As also depicted in Figure 1a, the region treated with the Ga-focused ion beam resulted in the MoS_2 growth, while no discernable feature was observed in the untreated regions. It is noteworthy that the sparse nucleation outside the pattern can likely be attributed to background levels of isolated hydroxyl groups, which provide some active sites for the MoS_2 nucleation (Figure 1b).

To uncover the association of the surface hydroxylation with the MoS_2 growth, an amorphous silica surface was first modeled by annealing of SiO_2 gas-phase molecules at an elevated temperature in the ReaxFF MD environment (Figure 2). This consists of the dehydroxylated region with Si–O dangling bonds (Figure 2a,e) and fully passivated siloxane (Figure 2a, b, and f). Then, the hydroxylated silica model (Figure 2b,g) was obtained by exposure of the amorphous silica surface in Figure 2a to H_2 gas molecules to passivate the O dangling bonds. As evident from Figure 2c,d the total bond orders of Si, O, and H atoms are accumulated around 4, 2, and 1, respectively, in both surfaces with and without hydroxylation, indicating that all atoms are fully coordinated and that the system does not have any radical sites.

The dehydroxylated and hydroxylated silica substrates were further treated (i) only with MoO_3, (ii) only with sulfur or H_2S, and (iii) in MoO_3 and sulfur (and H_2S) together as discussed in the following sections.

4.1. MoO_3 Nucleation on Silica. The scanning electron microscopy (SEM) image of the sample that was exposed only to MoO_3 shows that the Ga^+ ion-dosed region (with the red rectangle in Figure 3a,b) is densely covered with Mo species, but

https://doi.org/10.1021/acs.jpcc.3c01010
J. Phys. Chem. C 2023, 127, 9039–9048

the outside of the pattern indicated by the blue rectangle in Figure 3a,c shows no discernable feature. These results are consistent with ReaxFF simulations, which further confirm that the hydroxylated support is densely covered with MoO_3 molecules owing to the existence of OH groups on the surface (Figure 3d), while the fully coordinated siloxane surface remains inert during the MoO_3 flow over the course of the simulation (Figure 3e).

On the basis of the ReaxFF simulations, silanol groups formed on the surface after the Ga ion bombardment interact with MoO_3, leading to the reaction $MoO_3 + Si(OH)_4 \rightarrow (OH)\text{-}O_2Mo\text{-}OSi(OH)_3$. As illustrated in Figure 4d, MoO_3 approaching the surface interacts with H of the OH group, forming a transition state (Figure 4e). Then, the H atom leaves an O−Si dangling bond (O_{Si}) behind and intercalates into MoO_3, leading to the increase in the number of O−H in MoO_3 (O_{Mo}−H), as evidenced by the partial radial distribution functions in Figure 4b,c. This triggers the evolution of the Mo^{+6} state into Mo^{+5} (Figure 4f). Finally, the higher intermediate Mo^{+5} state interacts with O of the O═$Si(OH)_3$ group, thus initiating the nucleation of MoO_3 on the silica surface.

As seen from Figure 5a, such a reaction between MoO_3 and the hydroxylated silica surface is thermodynamically driven with

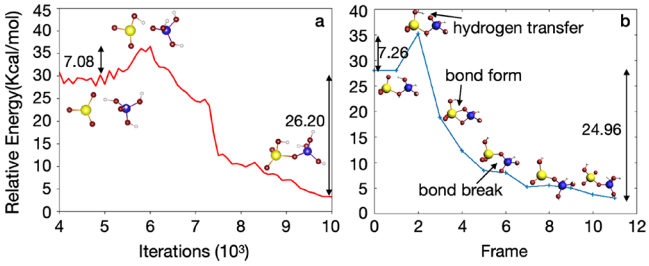

Figure 5. (a) ReaxFF and (b) DFT-based reaction pathway of MoO_3 protonation in the proximity of the silanol group. Note that the plot in (a) does not display the first 4000 iterations for a better comparison of ReaxFF with DFT.

the Gibbs free energy of −26.2 kcal/mol at the ReaxFF level. In addition, the H transfer from silanol to MoO_3 requires overcoming a kinetic barrier of 7.08 kcal/mol and is practically irreversible with a reverse barrier of 33.28 kcal/mol, which are in a good agreement with the results from DFT calculations (Figure 5b), indicating that the synthesis of MoS_2 on hydroxylated silica can be also kinetically driven at room temperature.

Another interesting result drawn from SEM images is that the extent of the MoO_3 growth is directly impacted by the Ga^+ ion beam dosage (compare regions I and II with 1.44×10^{16} and 5×10^{15} ions/cm^2, respectively, in Figure 6a). This result is connected to the ReaxFF simulations, which confirm that the surface reactivity toward MoO_3 is tunable and depends on the concentration of terminal OH groups (Figure 6b). The higher terminal OH group concentration yields the higher surface coverage rate by MoO_3 (compare Figure 6b-I with a high OH concentration of 0.84 mole/nm^3 to Figure 6b-II with a low OH concentration of 0.47 mole/nm^3). These results show the benefit of surface patterning for controlling and promoting the MoS_2 growth by generating Si−OH bond active sites on the surface for MoO_x absorbents, thereby initiating the nucleation of the MoS_2 epilayer. ReaxFF simulations further reveal that the non-Ga-treated silica surface utilized in the experiments should exhibit nonreactive character toward MoO_3 (Figure 3e), while O-terminated dehydroxylated silica is found chemically responsive to MoO_3 precursors only in the presence of dangling O−Si bonds on the surface (Figure S2e) as also confirmed by the DFT calculations presented in Figure S3. The MoO_3 interaction with the nonpassivated oxidized surface is the strongest with a binding energy of 3.78 eV (Figure S3c) followed by that with the hydroxylated surface with a binding energy of 3.05 eV (Figure S3b). The MoO_3 binding to the fully passivated siloxane is found the weakest with a binding energy of 1.77 eV (Figure S3a). All these results together indicate that the surface prior to the Ga treatment should compose of mainly 2-fold coordinated O atoms, which should be connected to each other by 4-fold coordinated Si atoms as in Figure 2f in order to maintain nonreactive character toward the precursors.

4.2. S_2 and H_2S Interactions with OH-Functionalized SiO_2. Our experimental results show that in the case of treating the silica surface only in a chalcogen precursor (S powder or H_2S), the surface reactivity of silica toward S powder alone is not influenced by the Ga treatment since no ion beam feature is observed on both untreated (light gray) and treated (dark gray) regions in Figure 7a and Figure S4. This observation is explained by ReaxFF simulations in Figure 7c,d where the light gray-colored dehydroxylated and hydroxylated SiO_2 surfaces are featureless because S_2 molecules stay inert at 2000 K and do not incorporate in the substrate regardless of the surface hydroxylation as also illustrated in Figure 7e,f. This is evidenced

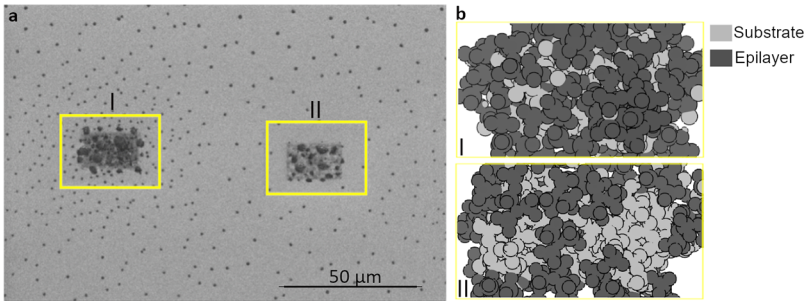

Figure 6. (a) SEM image of the silica surface with two areas treated with Ga^+ ion (highlighted with yellow rectangles) and tube furnace growth at 750 °C for 1 min at the peak temp. with MoO_3 powder only. The dark gray rectangle regions I and II (highlighted with yellow rectangles) are treated with the Ga^+ ion doses of 1.44×10^{16} and 5×10^{15} ions/cm^2, respectively. (b) ReaxFF-predicted MoO_3 nucleation on the surface with high (I) and low (II) −OH concentrations of 0.84 and 0.47 mole/nm^3, respectively, where the surface atoms (Si, O, and H) are colored with light gray and the precursors (MoO_x) are represented with dark gray balls as in SEM images.

https://doi.org/10.1021/acs.jpcc.3c01010
J. Phys. Chem. C 2023, 127, 9039−9048

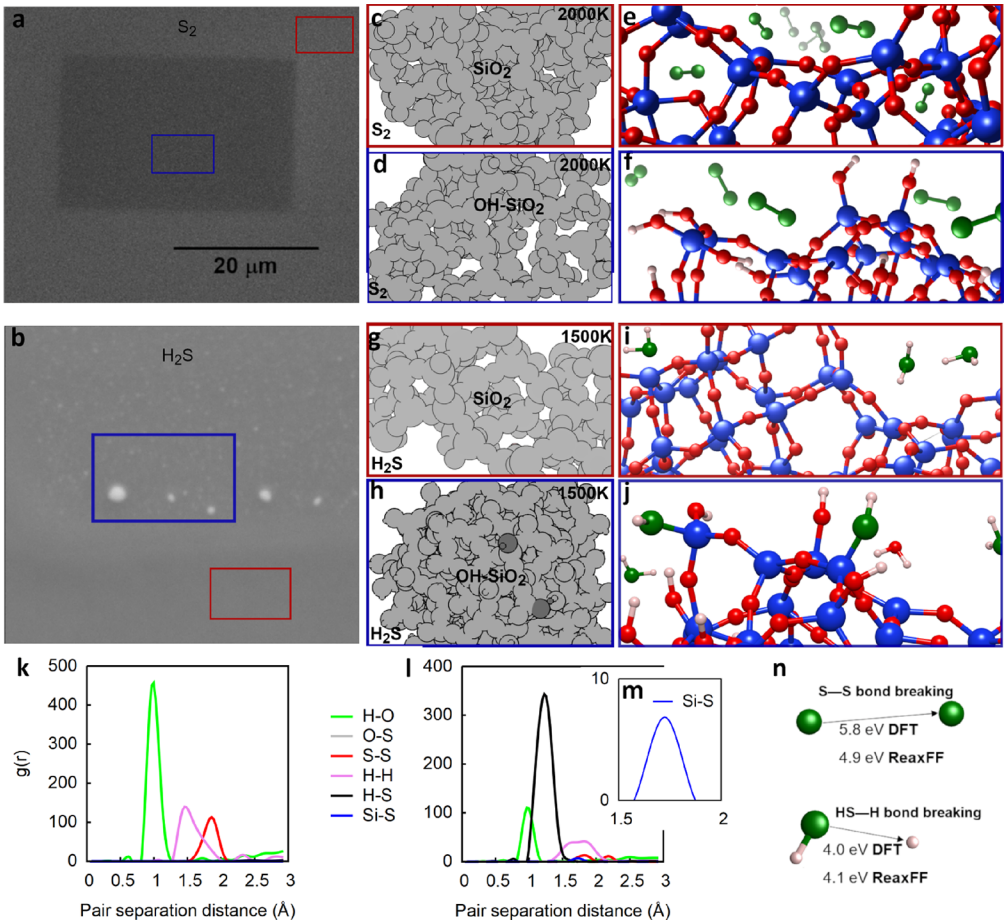

Figure 7. FESEM image of the samples that are exposed to (a) sulfur powder only showing no growth and (b) H_2S only showing features. Note that the color difference is only charge contrast in the SEM. Regions with/without Ga^+ ion irradiation in a and b are indicated with blue and red rectangles, respectively. Comparative ReaxFF MD snapshots of (c, e, g, and i) dehydroxylated siloxane and (d, f, h, and j) hydroxylated silica surfaces exposed to (c–f) S_2 at 2000 K and (g–j) H_2S at 1500 K for 2.5 ns. Note that, in c, d, g, and h, silica surfaces and S pattern formation are colored with light and dark gray, respectively, to match SEM images. (k,l) Partial radial distribution functions of bonds of interest in systems in f and j and (m) magnified portion of the graph in l. (n) Comparative S–S and H–SH bond breaking in S_2 and H_2S, respectively, at ReaxFF and DFT levels.

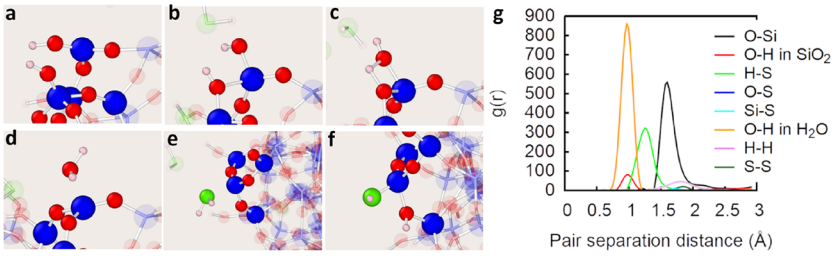

Figure 8. (a–d) Deprotonation of the silica surface resulting in water release, (e) proximal H_2S to the surface, and (f) HS– radical binding at 1500 K. (g) Radial distribution functions of the H_2S and MoO_3 system at 1500 K.

by the partial radial distribution functions in Figure 7k where there is no O–S signal observed at T = 2000 K.

However, after 5 min of H_2S treatment, the surface morphology inside the Ga-implanted patterns is altered (see the details in the Supporting Information (SI) and methods section, Figure 7b and Figure S4c) and exhibits a bumpy texture under the secondary electron mode compared to the relatively smooth area outside of the patterns, while the fully passivated dehydroxylated silica surface stays inert under H_2S exposure (Figure 7g,i), indicating the modification of the Ga-implanted silica surface under H_2S. Compared to S_2, the relatively low dissociation temperature of H_2S on the hydroxylated silica surface (i.e., 1500 K, Figure 6h where the HS pattern formation is highlighted with a dark gray color and Figure 7j) can be attributed to the fact that the S_2 dimer is a much more stable molecule in this chemical environment than the H_2S molecule. The energy required to break the S–S bond is higher than that for the HS–H bond (Figure 7n).

The ReaxFF predicted elemental steps of the HS pattern formation on the silica surface as follows: H_2S molecules stay inert at 1000 K as depicted by the partial radial distributions in Figure S5b. They start to decompose to HS– radicals at T = 1500 K (Figure 7l,m). In the meantime, the surface migration of H occurs between O atoms on the silica surface (Figure 8a–c).

https://doi.org/10.1021/acs.jpcc.3c01010
J. Phys. Chem. C 2023, 127, 9039–9048

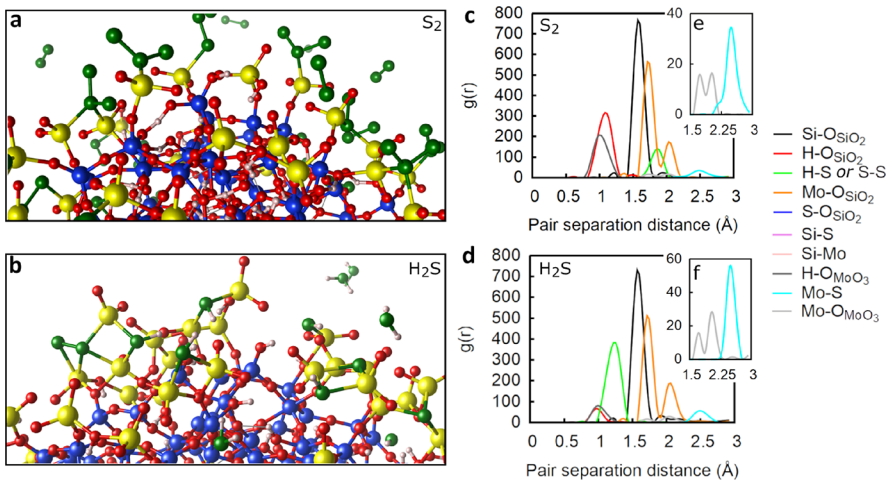

Figure 9. Hydroxylated silica surfaces exposed to (a) MoO_3 and S_2 and (b) MoO_3 and H_2S molecules at 1000 K in the ReaxFF MD environment and their partial radial distribution functions: (c) MoO_3 and S_2 and (d) MoO_3 and H_2S and (e,f) magnified portions of graphs in c and d showing the Mo−O and Mo−S bond distribution after annealing.

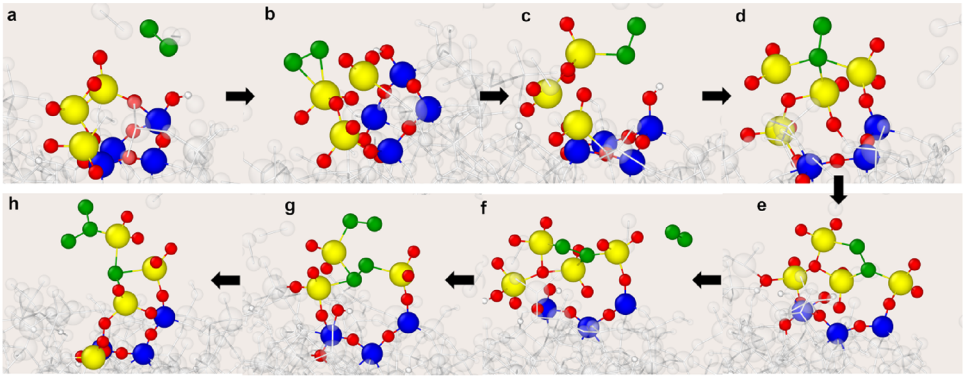

Figure 10. ReaxFF-predicted elementary steps of the MoS_2 nucleation process where (a) an S_2 molecule approaches the MoO_x-functionalized silica surface and (b−h) interacts with the Mo surface atoms.

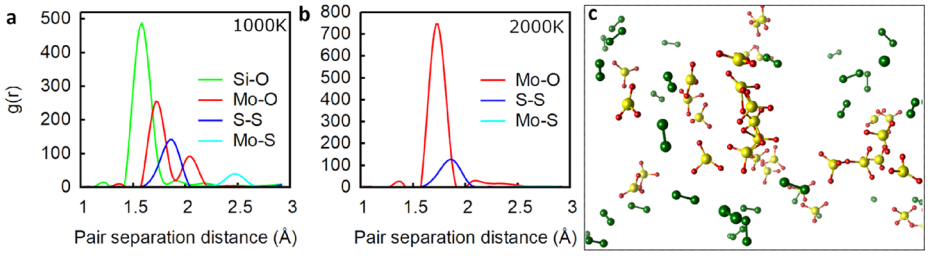

Figure 11. Gas-phase reactions of MoO_3 with S_2 in the presence of silica at (a) 1000 K and (b) in the absence of silica at 2000 K. (c) Representative ReaxFF MD snapshot of a MoO_3 and S_2 gas-phase system (without silica), which is annealed at 2000 K for 2.5 ns.

This leads to the water release by breaking the Si−O bond on the surface, resulting in an increase in the concentration of surface Si dangling bonds (Figure 8d), as also supported by the partial radial distribution function in Figure 8g. Then, the deprotonation of the silica surface is followed by the HS incorporation in the silica surface at 1500 K (Figure 8e).

4.3. Catalytic Effect of the Substrate on MoS_2 Nucleation. As shown in Figure 7 and Figure S1 and discussed in the previous section, chalcogen precursors (i.e., H_2S and S_2) are unable to attach to the silica surface at moderate temperatures (<1500 K) regardless of hydroxylation. In the case of simultaneous exposure of the hydroxylated surface to MoO_3 and chalcogen precursors, the surface functionalization by the MoO_x groups is followed by chalcogen binding, leading to the MoS_2 nucleation at moderate temperatures such as 1000 K (Figure 9a,b).

The comparative partial radial distribution functions at 1000 K (Figure 9c,d) further justify that no S−O_{Si} signal is achieved from the simulations, as also shown in Figure S5c,d, signifying that there is no S incorporation into the hydroxylated silica surface while the Mo−O_{Si} and Mo−S bond formations occur on the surface (Figure 9e,f). This indicates that the MoS_2 growth on the hydroxylated silica support initiates with the MoO_3 nucleation; in other words, the MoO_x-functionalized silica surface is a crucial factor in the chalcogen−surface interaction that triggers the growth of MoS_2. As highlighted by the potential elementary steps of the MoS_2 nucleation process in Figure 10, a S_2 molecule approaches to the MoO_x-functionalized silica

https://doi.org/10.1021/acs.jpcc.3c01010
J. Phys. Chem. C 2023, 127, 9039−9048

surface (Figure 10a) and interacts with the Mo surface atoms. Then, the S transfer occurs between S_2 surface groups, which leads to the Mo−S−Mo bond formation (Figure 10h). This indicates that the nucleation of MoS_2 is ruled by the chemical reactions occurring at the interface of the MoS_2 epilayer and the underlying substrate.

Figures 9−11 together also illuminate the catalytic role of silica in the reaction of metal and chalcogen precursors on the surface. The presence of silanol groups on silica promotes the surface reactions, leading to the MoS_2 nucleation at lower temperatures, as much as 1000 K, as confirmed by partial radial distribution functions in Figures 9c,d and 11a. However, S_2 precursors stay inert and do not interact with MoO_3 even at 2000 K in the absence of the substrate (Figure 11b,c). This signifies that the utilization of a substrate during the growth provides an effective way for energy saving and cost reduction in the MoS_2 fabrication, also driving the 2D nature of a material grown on a substrate.

5. CONCLUSIONS

In summary, using ReaxFF simulations, DFT calculations, and experimental growth, this work provides insights into the interplay between the surface chemistry and MoS_2 nucleation. We characterized and quantitatively demonstrated the intricate role of surface patterning in the MoS_2 nucleation. Our results show that owing to the tunable surface chemistry of silica, the surface reactivity can be interchanged between a reactive and nonreactive character depending on the concentration of the OH functional group. The fully saturated non-Ga^+-treated surface stays inert during exposure of metal and chalcogen precursors, while the Ga^+ treatment profoundly enhances the MoS_2 nucleation as a result of the presence of isolated Si−OH groups that occur in the thermally grown silicon oxide at a low density. The −OH groups formed after Ga^+ exposure generate active sites on the surface for metal reactants (e.g., MoO_3), kinetically and thermodynamically driving surface interactions between silica and precursors, signifying the benefit of surface engineering for controlling growth. Additionally, the reaction of the surface with MoO_3 initiates the nucleation of the MoS_2 epilayer, which is evidenced also by the partial radial distribution functions. Additionally, we find that the MoO_x-functionalized silica surface is an essential step to the chalcogen−surface interaction to initiate the MoS_2 growth. The conclusions drawn in this work provide a fundamental understanding of patterning nucleation sites on a silicon dioxide substrate to promote the spatial growth of large-area monolayer MoS_2.

■ ASSOCIATED CONTENT

Supporting Information

The Supporting Information is available free of charge at https://pubs.acs.org/doi/10.1021/acs.jpcc.3c01010.

ReaxFF reactive force field parameters for Mo/O/Si/H/S interactions (TXT)

Comparative DFT and ReaxFF results for nonperiodic and periodic calculations included in the training set (PDF)

■ AUTHOR INFORMATION

Corresponding Author

Adri C. T. van Duin − *2D Crystal Consortium Material Innovation Platform (2DCC-MPI) Materials Research Institute and Department of Mechanical Engineering, The Pennsylvania State University, University Park, Pennsylvania 16802, United States;* orcid.org/0000-0002-3478-4945; Email: acv13@psu.edu

Authors

Nadire Nayir − *Department of Physics, Karamanoglu Mehmetbey University, Karaman 70000, Turkey; 2D Crystal Consortium Material Innovation Platform (2DCC-MPI) Materials Research Institute and Department of Mechanical Engineering, The Pennsylvania State University, University Park, Pennsylvania 16802, United States;* orcid.org/0000-0002-3621-2481

Stephen Bartolucci − *U.S. Army Combat Capabilities Development Command Armaments Center, Watervliet, New York 12189, United States*

Tao Wang − *Department of Mechanical Engineering, The Pennsylvania State University, University Park, Pennsylvania 16802, United States*

Chen Chen − *Department of Materials Science and Engineering, The Pennsylvania State University, University Park, Pennsylvania 16802, United States*

Joshua Maurer − *U.S. Army Combat Capabilities Development Command Armaments Center, Watervliet, New York 12189, United States;* orcid.org/0000-0002-6663-0721

Joan M. Redwing − *2D Crystal Consortium Material Innovation Platform (2DCC-MPI) Materials Research Institute and Department of Materials Science and Engineering, The Pennsylvania State University, University Park, Pennsylvania 16802, United States;* orcid.org/0000-0002-7906-452X

Complete contact information is available at: https://pubs.acs.org/10.1021/acs.jpcc.3c01010

Author Contributions

The manuscript was written through the contributions of all authors. All authors have given approval to the final version of the manuscript.

Funding

The National Science Foundation (NSF) through the Pennsylvania State University 2D Crystal Consortium−Materials Innovation Platform (2DCC-MIP) under NSF cooperative agreements DMR-1539916 and DMR-2039351.

Notes

The authors declare no competing financial interest.

■ ACKNOWLEDGMENTS

The work was financially supported by the National Science Foundation (NSF) through the Pennsylvania State University 2D Crystal Consortium−Materials Innovation Platform (2DCC-MIP) under NSF cooperative agreements DMR-1539916 and DMR-2039351.

■ REFERENCES

(1) Radisavljevic, B.; Radenovic, A.; Brivio, J.; Giacometti, V.; Kis, A. Single-Layer MoS 2 Transistors. *Nat. Nanotechnol.* **2011**, *6*, 147−150.

(2) Splendiani, A.; Sun, L.; Zhang, Y.; Li, T.; Kim, J.; Chim, C.-Y.; Galli, G.; Wang, F. Emerging Photoluminescence in Monolayer MoS2. *Nano Lett.* **2010**, *10*, 1271−1275.

(3) Wu, S.; Ross, J. S.; Liu, G.-B.; Aivazian, G.; Jones, A.; Fei, Z.; Zhu, W.; Xiao, D.; Yao, W.; Cobden, D.; et al. Electrical Tuning of Valley Magnetic Moment through Symmetry Control in Bilayer MoS2. *Nat. Phys.* **2013**, *9*, 149−153.

(4) Xiao, D.; Liu, G.-B.; Feng, W.; Xu, X.; Yao, W. Coupled Spin and Valley Physics in Monolayers of MoS2 and Other Group-VI Dichalcogenides. *Phys. Rev. Lett.* **2012**, *108*, No. 196802.
(5) Zhang, W.; Wang, Q.; Chen, Y.; Wang, Z.; Wee, A. T. S. Van Der Waals Stacked 2D Layered Materials for Optoelectronics. *2D Mater.* **2016**, *3*, No. 022001.
(6) Backes, C.; Higgins, T. M.; Kelly, A.; Boland, C.; Harvey, A.; Hanlon, D.; Coleman, J. N. Guidelines for Exfoliation, Characterization and Processing of Layered Materials Produced by Liquid Exfoliation. *Chem. Mater.* **2017**, *29*, 243−255.
(7) Magda, G. Z.; Pető, J.; Dobrik, G.; Hwang, C.; Biró, L. P.; Tapasztó, L. Exfoliation of Large-Area Transition Metal Chalcogenide Single Layers. *Sci. Rep.* **2015**, *5*, 14714.
(8) Synnatschke, K.; Cieslik, P. A.; Harvey, A.; Castellanos-Gomez, A.; Tian, T.; Shih, C.-J.; Chernikov, A.; Santos, E. J. G.; Coleman, J. N.; Backes, C. Length- and Thickness-Dependent Optical Response of Liquid-Exfoliated Transition Metal Dichalcogenides. *Chem. Mater.* **2019**, *31*, 10049−10062.
(9) Lukowski, M. A.; Daniel, A. S.; Meng, F.; Forticaux, A.; Li, L.; Jin, S. Enhanced Hydrogen Evolution Catalysis from Chemically Exfoliated Metallic MoS2 Nanosheets. *J. Am. Chem. Soc.* **2013**, *135*, 10274−10277.
(10) Dumcenco, D.; Ovchinnikov, D.; Marinov, K.; Lazić, P.; Gibertini, M.; Marzari, N.; Sanchez, O. L.; Kung, Y.-C.; Krasnozhon, D.; Chen, M.-W.; et al. Large-Area Epitaxial Monolayer MoS2. *ACS Nano* **2015**, *9*, 4611−4620.
(11) Lee, Y.-H.; Zhang, X.-Q.; Zhang, W.; Chang, M.-T.; Lin, C.-T.; Chang, K.-D.; Yu, Y.-C.; Wang, J. T.-W.; Chang, C.-S.; Li, L.-J.; et al. Synthesis of Large-Area MoS2 Atomic Layers with Chemical Vapor Deposition. *Adv. Mater.* **2012**, *24*, 2320−2325.
(12) Chiu, M.-H.; Zhang, C.; Shiu, H.-W.; Chuu, C.-P.; Chen, C.-H.; Chang, C.-Y. S.; Chen, C.-H.; Chou, M.-Y.; Shih, C.-K.; Li, L.-J. Determination of Band Alignment in the Single-Layer MoS2/WSe2 Heterojunction. *Nat. Commun.* **2015**, *6*, 7666.
(13) Joon Pyeon, J.; Hyun Kim, S.; Seok Jeong, D.; Baek, S.-H.; Kang, C.-Y.; Kim, J.-S.; Keun Kim, S. Wafer-Scale Growth of MoS 2 Thin Films by Atomic Layer Deposition. *Nanoscale* **2016**, *8*, 10792−10798.
(14) Bartolucci, S. F.; Kaplan, D.; Maurer, J. A. Ion Beam-Induced Hydroxylation Controls Molybdenum Disulfide Growth. *2D Mater.* **2017**, *4*, No. 021017.
(15) Zhu, D.; Shu, H.; Jiang, F.; Lv, D.; Asokan, V.; Omar, O.; Yuan, J.; Zhang, Z.; Jin, C. Capture the Growth Kinetics of CVD Growth of Two-Dimensional MoS 2. *Npj 2D Mater. Appl.* **2017**, *1*, 1−8.
(16) Najmaei, S.; Liu, Z.; Zhou, W.; Zou, X.; Shi, G.; Lei, S.; Yakobson, B. I.; Idrobo, J.-C.; Ajayan, P. M.; Lou, J. Vapour Phase Growth and Grain Boundary Structure of Molybdenum Disulphide Atomic Layers. *Nat. Mater.* **2013**, *12*, 754−759.
(17) Momeni, K.; Ji, Y.; Nayir, N.; Sakib, N.; Zhu, H.; Paul, S.; Choudhury, T. H.; Neshani, S.; van Duin, A. C. T.; Redwing, J. M.; et al. A Computational Framework for Guiding the MOCVD-Growth of Wafer-Scale 2D Materials. *npj Comput. Mater.* **2022**, *8*, 1−8.
(18) Momeni, K.; Ji, Y.; Nayir, N.; Sakib, N.; Zhu, H.; Paul, S.; Choudhury, T. H.; Neshani, S.; van Duin, A. C. T.; Redwing, J. M.; et al. Author Correction: A Computational Framework for Guiding the MOCVD-Growth of Wafer-Scale 2D Materials. *npj Comput. Mater.* **2022**, *8*, 1−1.
(19) Momeni, K.; Ji, Y.; Zhang, K.; Robinson, J. A.; Chen, L.-Q. Multiscale Framework for Simulation-Guided Growth of 2D Materials. *Npj 2D Mater. Appl.* **2018**, *2*, 1−7.
(20) Momeni, K.; Ji, Y.; Wang, Y.; Paul, S.; Neshani, S.; Yilmaz, D. E.; Shin, Y. K.; Zhang, D.; Jiang, J.-W.; Park, H. S.; et al. Multiscale Computational Understanding and Growth of 2D Materials: A Review. *npj Comput. Mater.* **2020**, *6*, 1−18.
(21) Paul, S.; Torsi, R.; Robinson, J. A.; Momeni, K. Effect of the Substrate on MoS2 Monolayer Morphology: An Integrated Computational and Experimental Study. *ACS Appl. Mater. Interfaces* **2022**, *14*, 18835−18844.
(22) Li, X.; Zhang, S.; Chen, S.; Zhang, X.; Gao, J.; Zhang, Y.-W.; Zhao, J.; Shen, X.; Yu, R.; Yang, Y.; et al. Mo Concentration Controls the Morphological Transitions from Dendritic to Semicompact, and to Compact Growth of Monolayer Crystalline MoS2 on Various Substrates. *ACS Appl. Mater. Interfaces* **2019**, *11*, 42751−42759.
(23) Margulis, L.; Salitra, G.; Tenne, R.; Talianker, M. Nested Fullerene-like Structures. *Nature* **1993**, *365*, 113−114.
(24) Feldman, Y.; Wasserman, E.; Srolovitz, D. J.; Tenne, R. High-Rate, Gas-Phase Growth of MoS2 Nested Inorganic Fullerenes and Nanotubes. *Science* **1995**, 222.
(25) Weber, T.; Muijsers, J. C.; van Wolput, J. H. M. C.; Verhagen, C. P. J.; Niemantsverdriet, J. W. Basic Reaction Steps in the Sulfidation of Crystalline MoO3 to MoS2, As Studied by X-Ray Photoelectron and Infrared Emission Spectroscopy. *J. Phys. Chem.* **1996**, *100*, 14144−14150.
(26) Li, X. L.; Li, Y. D. Formation of MoS2 Inorganic Fullerenes (IFs) by the Reaction of MoO3 Nanobelts and S. *Chem. − Eur. J.* **2003**, *9*, 2726−2731.
(27) Van Der Zande, A. M.; Huang, P. Y.; Chenet, D. A.; Berkelbach, T. C.; You, Y.; Lee, G.-H.; Heinz, T. F.; Reichman, D. R.; Muller, D. A.; Hone, J. C. Grains and Grain Boundaries in Highly Crystalline Monolayer Molybdenum Disulphide. *Nat. Mater.* **2013**, *12*, 554−561.
(28) Song, X. C.; Zhao, Y.; Zheng, Y. F.; Yang, E. Large-Scale Synthesis of MoS2 Bucky Onions. *Adv. Eng. Mater.* **2007**, *9*, 96−98.
(29) Chen, J.; Tang, W.; Tian, B.; Liu, B.; Zhao, X.; Liu, Y.; Ren, T.; Liu, W.; Geng, D.; Jeong, H. Y.; et al. Chemical Vapor Deposition of High-Quality Large-Sized MoS2 Crystals on Silicon Dioxide Substrates. *Adv. Sci.* **2016**, *3*, 1500033.
(30) Chang, M.-C.; Ho, P.-H.; Tseng, M.-F.; Lin, F.-Y.; Hou, C.-H.; Lin, I.-K.; Wang, H.; Huang, P.-P.; Chiang, C.-H.; Yang, Y.-C.; et al. Fast Growth of Large-Grain and Continuous MoS2 Films through a Self-Capping Vapor-Liquid-Solid Method. *Nat. Commun.* **2020**, *11*, 3682.
(31) Wan, Y.; Zhang, H.; Zhang, K.; Wang, Y.; Sheng, B.; Wang, X.; Dai, L. Large-Scale Synthesis and Systematic Photoluminescence Properties of Monolayer MoS2 on Fused Silica. *ACS Appl. Mater. Interfaces* **2016**, *8*, 18570−18576.
(32) Jeon, J.; Jang, S. K.; Jeon, S. M.; Yoo, G.; Jang, Y. H.; Park, J.-H.; Lee, S. Layer-Controlled CVD Growth of Large-Area Two-Dimensional MoS2 Films. *Nanoscale* **2015**, *7*, 1688−1695.
(33) Ling, X.; Lee, Y.-H.; Lin, Y.; Fang, W.; Yu, L.; Dresselhaus, M. S.; Kong, J. Role of the Seeding Promoter in MoS2 Growth by Chemical Vapor Deposition. *Nano Lett.* **2014**, *14*, 464−472.
(34) Ko, D.-S.; Park, Y. M.; Kim, S.-D.; Kim, Y.-W. Effective Removal of Ga Residue from Focused Ion Beam Using a Plasma Cleaner. *Ultramicroscopy* **2007**, *107*, 368−373.
(35) Tsafack, T.; Bartolucci, S. F.; Maurer, J. A. The Role of Molybdenum Oxysulfide Rings in the Formation of Two-Dimensional Molybdenum Disulfide by Powder Vaporization. *J. Phys. Chem. A* **2018**, *122*, 7320−7327.
(36) Tsafack, T.; Bartolucci, S. F.; Maurer, J. A. Elucidation of Molybdenum Trioxide Sulfurization: Mechanistic Insights into Two-Dimensional Molybdenum Disulfide Growth. *J. Phys. Chem. A* **2021**, *125*, 1809−1815.
(37) Ostadhossein, A.; Rahnamoun, A.; Wang, Y.; Zhao, P.; Zhang, S.; Crespi, V. H.; van Duin, A. C. T. ReaxFF Reactive Force-Field Study of Molybdenum Disulfide (MoS_2). *J. Phys. Chem. Lett.* **2017**, *8*, 631−640.
(38) Yogev, S.; Levin, J.; Molotskii, M.; Schwarzman, A.; Avayu, O.; Rosenwaks, Y. Charging of Dielectrics under Focused Ion Beam Irradiation. *J. Appl. Phys.* **2008**, *103*, No. 064107.
(39) Van Duin, A. C. T.; Dasgupta, S.; Lorant, F.; Goddard, W. A. ReaxFF: A Reactive Force Field for Hydrocarbons. *J. Phys. Chem. A* **2001**, *105*, 9396−9409.
(40) Chenoweth, K.; van Duin, A. C. T.; Goddard, W. A. ReaxFF Reactive Force Field for Molecular Dynamics Simulations of Hydrocarbon Oxidation. *J. Phys. Chem. A* **2008**, *112*, 1040−1053.
(41) Mortier, W. J.; Ghosh, S. K.; Shankar, S. Electronegativity-Equalization Method for the Calculation of Atomic Charges in Molecules. *J. Am. Chem. Soc.* **1986**, *108*, 4315−4320.
(42) Nayir, N.; Wang, Y.; Ji, Y.; Choudhury, T. H.; Redwing, J. M.; Chen, L.-Q.; Crespi, V. H.; van Duin, A. C. T. Theoretical Modeling of

https://doi.org/10.1021/acs.jpcc.3c01010
J. Phys. Chem. C 2023, 127, 9039−9048

Edge-Controlled Growth Kinetics and Structural Engineering of 2D-MoSe2. *Mater. Sci. Eng., B* **2021**, *271*, No. 115263.
(43) Nayir, N.; Shin, Y. K.; Wang, Y.; Sengul, M. Y.; Hickey, D. R.; Chubarov, M.; Choudhury, T. H.; Alem, N.; Redwing, J.; Crespi, V. H.; et al. A ReaxFF Force Field for 2D-WS2 and Its Interaction with Sapphire. *J. Phys. Chem. C* **2021**, *125*, 17950−17961.
(44) Nayir, N.; Wang, Y.; Shabnam, S.; Hickey, D. R.; Miao, L.; Zhang, X.; Bachu, S.; Alem, N.; Redwing, J.; Crespi, V. H.; et al. Modeling for Structural Engineering and Synthesis of Two-Dimensional WSe2 Using a Newly Developed ReaxFF Reactive Force Field. *J. Phys. Chem. C* **2020**, *124*, 28285−28297.
(45) Reifsnyder Hickey, D.; Nayir, N.; Chubarov, M.; Choudhury, T. H.; Bachu, S.; Miao, L.; Wang, Y.; Qian, C.; Crespi, V. H.; Redwing, J. M.; et al. Illuminating Invisible Grain Boundaries in Coalesced Single-Orientation WS2 Monolayer Films. *Nano Lett.* **2021**, *21*, 6487−6495.
(46) Xuan, Y.; Jain, A.; Zafar, S.; Lotfi, R.; Nayir, N.; Wang, Y.; Choudhury, T. H.; Wright, S.; Feraca, J.; Rosenbaum, L.; et al. Multi-Scale Modeling of Gas-Phase Reactions in Metal-Organic Chemical Vapor Deposition Growth of WSe2. *J. Cryst. Growth* **2019**, *527*, No. 125247.
(47) Rajabpour, S.; Mao, Q.; Nayir, N.; Robinson, J. A.; van Duin, A. C. T. Development and Applications of ReaxFF Reactive Force Fields for Group-III Gas-Phase Precursors and Surface Reactions with Graphene in Metal−Organic Chemical Vapor Deposition Synthesis. *J. Phys. Chem. C* **2021**, *125*, 10747−10758.
(48) Lotfi, R.; Naguib, M.; Yilmaz, D. E.; Nanda, J.; Van Duin, A. C. T. A Comparative Study on the Oxidation of Two-Dimensional Ti3C2 MXene Structures in Different Environments. *J. Mater. Chem. A* **2018**, *6*, 12733−12743.
(49) Kowalik, M.; Hossain, M. J.; Lele, A.; Zhu, W.; Banerjee, R.; Granzier-Nakajima, T.; Terrones, M.; Hudson, E. W.; van Duin, A. C. T. Atomistic-Scale Simulations on Graphene Bending Near a Copper Surface. *Catalysts* **2021**, *11*, 208.
(50) Gao, Z.; Zhu, J.; Rajabpour, S.; Joshi, K.; Kowalik, M.; Croom, B.; Schwab, Y.; Zhang, L.; Bumgardner, C.; Brown, K. R.; et al. Graphene Reinforced Carbon Fibers. *Sci. Adv.* **2020**, *6*, No. eaaz4191.
(51) Berendsen, H. J. C.; Postma, J. P. M.; van Gunsteren, W. F.; DiNola, A.; Haak, J. R. Molecular Dynamics with Coupling to an External Bath. *J. Chem. Phys.* **1984**, *81*, 3684−3690.
(52) *Amsterdam Modeling Suite Making Computational Chemistry Work For You. Software for Chemistry & Materials*. https://www.scm.com/ (accessed 2020-11-10).
(53) Stukowski, A. Visualization and Analysis of Atomistic Simulation Data with OVITO−the Open Visualization Tool. *Modell. Simul. Mater. Sci. Eng.* **2009**, *18*, No. 015012.
(54) Momma, K.; Izumi, F. VESTA 3 for Three-Dimensional Visualization of Crystal, Volumetric and Morphology Data. *J. Appl. Crystallogr.* **2011**, *44*, 1272−1276.
(55) Bochevarov, A. D.; Harder, E.; Hughes, T. F.; Greenwood, J. R.; Braden, D. A.; Philipp, D. M.; Rinaldo, D.; Halls, M. D.; Zhang, J.; Friesner, R. A. Jaguar: A High-Performance Quantum Chemistry Software Program with Strengths in Life and Materials Sciences. *Int. J. Quantum Chem.* **2013**, *113*, 2110−2142.
(56) Velde, G.; Bickelhaupt, F. M.; Baerends, E. J.; Guerra, C. F.; Gisbergen, S. J. A.; Snijders, J. G.; Ziegler, T. Chemistry with ADF. *J. Comput. Chem.* **2001**, *22*, 931−967.
(57) Perdew, J. P.; Burke, K.; Ernzerhof, M. Generalized Gradient Approximation Made Simple. *Phys. Rev. Lett.* **1996**, *77*, 3865−3868.
(58) Kresse, G.; Furthmüller, J. Efficient Iterative Schemes for Ab Initio Total-Energy Calculations Using a Plane-Wave Basis Set. *Phys. Rev. B* **1996**, *54*, 11169−11186.
(59) Blöchl, P. E. Projector Augmented-Wave Method. *Phys. Rev. B* **1994**, *50*, 17953−17979.
(60) Kresse, G.; Joubert, D. From Ultrasoft Pseudopotentials to the Projector Augmented-Wave Method. *Phys. Rev. B* **1999**, *59*, 1758−1775.
(61) Perdew, J. P.; Burke, K.; Ernzerhof, M. Generalized Gradient Approximation Made Simple. *Phys. Rev. Lett.* **1997**, *78*, 1396−1396.
(62) Grimme, S.; Antony, J.; Ehrlich, S.; Krieg, H. A Consistent and Accurate Ab Initio Parametrization of Density Functional Dispersion Correction (DFT-D) for the 94 Elements H-Pu. *J. Chem. Phys.* **2010**, *132*, 154104.

https://doi.org/10.1021/acs.jpcc.3c01010
J. Phys. Chem. C 2023, 127, 9039−9048